Expansion of epileptogenic networks via neuroplasticity

Elif Köksal-Ersöz, Pascal Benquet, Fabrice Wendling

Expansion of epileptogenic networks via neuroplasticity

Elif Köksal-Ersöz[1], Pascal Benquet[1], Fabrice Wendling[1]

1 Univ Rennes, INSERM, LTSI UMR 1099, F-35000, Rennes, FRANCE

Abstract

Neuroplasticity refers to functional and structural changes in brain regions in response to healthy and pathological activity. Neuroplasticity induced by epileptic activity can involve healthy brain regions into the epileptogenic network by perturbing their excitation/inhibition balance. In this article, we present a new neural mass model that accounts for neuroplasticity and that is used to investigate the possible mechanisms underlying the epileptogenic network expansion. We formulate physiological calcium-mediated synaptic plasticity and pathological structural plasticity in a multiple-timescale framework. The model highlights that synaptic plasticity at excitatory connections and structural changes in the inhibitory system can transform a healthy region into a secondary epileptic focus under recurrent seizures and interictal activity occurring in the primary focus. Our results suggest that the latent period of this transformation can provide a window of opportunity to preventthe expansion of epileptogenic networks, formation of an epileptic focus, or other comorbidities associated with epileptic activity.

Key words: epilepsy, synaptic plasticity, secondary focus, neural mass model, multiple timescale systems

Author Summary

Repetitive epileptic activity leads to a large variety of plastic changes in brain. Understanding the mechanism and its time course can indicate windows of opportunity for preventing the devastating

impact of focal epileptic activity on brain networks. Animal models of focal epilepsy underlined to role of NMDA receptors and deregulations in the GABAergic system in the expansion of epileptic activity. Here we develop a plastic neural mass model integrating physiological and pathologic plasticity. Our results show that neuroplasticity mediated by epileptic activity increases synaptic efficacy between epileptic and healthy regions, and causes irreversible changes in the GABAergic system in the healthy region. The model gives mechanistic insights into the physio-pathological impact of focal epileptic activity on large-scale networks and suggests that seizures may beget seizures.

Introduction

The most general definition of neuroplasticity is the ability of neural networks to reorganize over time, which can take place under physiological and pathological conditions. Synaptic plasticity is the ability of synapses to strengthen or weaken, in response to increases or decreases in their activity. Under physiological conditions, it is accompanied by many regulatory mechanisms through which the excitation/inhibition balance is preserved (for examples [1–6]). However, epileptiform discharges drive not only physiologic synaptic plasticity but also pathological plasticity, which disturbs the excitation/inhibition balance, and can cause expansion of epileptogenic networks during epileptogenesis [7–9]. The aim of this article is to investigate the expansion of epileptogenic networks with a neurophysiologically plausible mathematical model of physio-pathological plasticity under recurrent epileptic activity.

Synaptic plasticity occurs on multiple timescales at both presynaptic and postsynaptic sites [10]. Short-term plasticity (STP, in milliseconds) refers to transient changes in the probability of neurotransmitter release at the presynaptic site [11]. Long-term synaptic plasticity (in hours or days), although generally considered as postsynaptic alterations, is related to both (i) the insertion/removal of alpha-amino-3-hydroxy-5-methyl-4-isoxazolepropionic acid (AMPA) receptors (AMPARs) at the postsynaptic site and (ii) the change in the probability of neurotransmitter release at the presynaptic site [12].

Postsynaptic long-term potentiation (LTP) and long-term depression (LTD) depend on the calcium concentration at the postsynaptic site [13]. In excitatory (glutamatergic) synapses, an increase in postsynaptic calcium concentration through activation of synaptic N-methyl-D-aspartate (NMDA) receptors (NMDARs), metabotropic glutamate receptors, voltage-gated calcium channels, etc. is necessary and sufficient for synaptic plasticity (see [12,14] and references therein). Calcium-dependent activation of secondary messengers, such as nitric oxide, endocannabinoids, etc., triggers presynaptic long-term plasticity [15,16]. The late phase of long-term plasticity, referred to as maintenance or consolidation, occurs via new protein synthesis and gene transcription [12].

Epileptic discharges that cause glutamatergic spillover have a twofold impact. First, epileptiform activity strengthens excitatory synapses by increasing the number of alpha-amino-3-hydroxy-5-methyl-4-isoxazolepropionic acid receptors (AMPARs) [17,18], as in the physiological LTP. Second, a high amount of glutamate released during epileptiform activity can activate extrasynaptic NMDARs that cause pathological changes in GABAergic signaling, through inactivation of functional potassium chloride co-transporters 2 (KCC2) and internalization of GABAergic receptors [19,20]. KCC2 controls the outflow of the chloride ions entered the intracellular space through GABAergic channels to the extracellular and maintains the GABAergic reversal potential. Calcium ions flowing through extrasynaptic NMDARs bind on calpain that inactivates KCC2 [20–22]. Reducing the number of functional KCC2 results in the increase of chloride concentration and changes GABAergic responses from inhibitory to excitatory. KCC2 dysfunction is related to epileptic activity in the naive site [7], and it is one of the factors contributing to epileptic activity in the mature brain [23].

The extrasynaptic NMDAR activity also affects tonic inhibition that is mainly mediated by the α_5GABA$_A$ receptors in the hippocampus. Overexpression of GluN2B NMDA receptors, which are located mostly in extrasynaptic regions, downregulates the expression of α_5GABA$_A$ receptors expression, promotes their internalization, and therefore, reduces tonic GABAergic [24] (but see [25] for limbic epileptogenesis). We

refer to these two mechanisms, i.e. reduced KCC2 and internalization of extrasynaptic GABAR, as *pathological plasticity*.

Physiological synaptic plasticity followed by pathological plasticity can increase the susceptibility of a brain region to epileptic discharges, expand epileptic network, and generate a secondary (mirror) focus. Secondary (mirror) focus refers to epileptogenesis in a naive area induced by repetitively uncontrolled epileptic seizures from a primary seizure focus [26,27]. Independent epileptic activity in the contralateral area in humans suggests that mirror focus develops via a kindling process mediated by the primary focus. In animal models of epilepsy, for instance, under kindling [28] or kainite application [7] to one of the hippocampi (primary focus), secondary focus appears in the contralateral hippocampus due to recurrent epileptic activity in the primary focus. Khalilov's elegant work in the immature brain [7] showed that activation of NMDARs and long-term alterations in GABAergic synapses are responsible for chronic epileptogenesis in the secondary focus. Despite the key role of plasticity in expansion of epileptogenic networks, there is a lack of computational modeling studies of neuroplasticity under epileptic activity.

Previous modeling studies of calcium-mediated postsynaptic LTP/LTD have mainly focused on cellular activity [29–34] (see [35] for a mean-field approximation), as well as presynaptic long-term plasticity [30,33,36,37]. Recently, Chindemi et al. [30] developed a detailed cellular model of the neocortex that integrates the calcium-mediated presynaptic and postsynaptic plasticity mechanisms. However, the literature related to modeling calcium-mediated plasticity with neuro-physiologically plausible neural mass model (NMMs) remains limited. We identified two studies on this phenomenon in the context of magnetic stimulation [38,39]. Our computational model concentrates on the physio-pathological plasticity under epileptic activity in a network of two unidirectionally coupled NMMs [40], each representing an epileptic and a non-epileptic brain region, where the epileptic one perturbs the non-epileptic one. First, we study how synaptic connections evolve under epileptic activity. We then investigate the pathological plasticity triggered by the physiological plasticity. The results suggest that the

interaction between physiological and pathological plasticity can explain the expansion of epileptogenic networks and the formation of secondary epileptic foci.

Methods

Mesoscopic model of physiological short- and long-term plasticity

The seminal study by Shouval et al. [29] has proposed a calcium control hypothesis for postsynaptic plasticity, in which intra-cellular calcium concentration controls the rate of change of synaptic efficacy. The proposed model in [29] was then developed to account for the synaptic consolidation in [32] by introducing a variable ρ that describes the state of the synaptic efficacy. We combine both formulations as:

$$\frac{d\rho}{dt} = \frac{1}{\tau_\rho}\left(-\rho(1-\rho)(\rho_* - \rho) + (1-\rho)\Omega_p([Ca]) - \rho\Omega_d([Ca])\right), \quad (1)$$

where τ_ρ is the time constant of the synaptic variations, $\rho_* = 0.5$ is the boundary between the depressed ($\rho = 0$) and potentiated ($\rho = 1$) states. The functions $\Omega_{p,d}([Ca])$ describe how the synaptic efficacy is controlled by the calcium concentration:

$$\Omega_{p,d}([Ca]) = \frac{\gamma_{p,d}}{1 + exp(-\beta_{p,d}([Ca] - \theta_{p,d}))}, \quad (2)$$

where $\gamma_p > \gamma_d$ are potentiation and depression rates, $\beta_{p,d}$ are the slopes and $\theta_p > \theta_d$ are potentiation and depression boundaries (Fig 1A).

Figure 1 Synaptic efficacy and activation functions. (A) Calcium dependent synaptic efficacy function, $\Omega([Ca]) = -\Omega_d([Ca]) + \Omega_p([Ca])$ (2) for. (B) Activation function, $H(V_{post})$ (5) the parameter set given in Table 1.

The calcium concentration is controlled by the NMDAR-mediated current $I_{NMDA}^{[Ca]}$:

$$\frac{d[Ca]}{dt} = I_{NMDA}^{[Ca]} - \frac{[Ca]}{\tau_{\{Ca\}}}, \quad (3)$$

where τ_{ca} is the decay time constant of calcium influx. The NMDAR-mediated calcium current $I_{NMDA}^{[Ca]}$ depend on both the presynaptic activity via the kinetics of glutamate binding and the postsynaptic membrane potential [29] expressed as,

$$I_{NMDA}^{[Ca]} = G(FR_{pre})h_{Ca}H(V_{post}), \tag{4}$$

where $G(FR_{pre})$ formulates the kinetics of the glutamate binding depending on the firing rate of the presynaptic population, FR_{pre}. The function $H(V_{post})$ (Fig. 1B) formulates the relation between the NMDA currents and the postsynaptic (population level) depolarization:

$$H(V_{post}) = \frac{1}{1 + exp\left(-\mu(V_{post} - V_{th})\right)}, \tag{5}$$

where μ is the slope at $V_{th} = V_{post}$. The function $H(V_{post})$ can be interpreted as the magnesium blockage at the population level. Parameter h_{Ca} is a scaling factor, which distinguishes the NMDAR-mediated postsynaptic depolarization from calcium entry.

Plasticity of excitatory synapses is modeled at both presynaptic and postsynaptic levels. Presynaptic plasticity corresponds to variations in glutamate release probability, running on short- and long-timescales. The presynaptic STP rule follows [41]:

$$\frac{dr}{dt} = \frac{1 - r}{\tau_r} - u\, r\, FR_{pre} \tag{6a}$$

$$\frac{du}{dt} = \frac{U_{se} - u}{\tau_f} + U_{se}(1 - u)FR_{pre} \tag{6b}$$

where r is the amount of available neurotransmitters, u is the utilization factor, τ_r is the recovery timescale, τ_f is the facilitation timescale and U_{se} is the neurotransmitter release probability.

The presynaptic long-term plasticity is the long-term variations in the neurotransmitter release probability U_{se} controlled by the calcium-dependent retrograde signaling [30],

$$\frac{dU_{se}}{dt} = \frac{1}{\tau_{Use}}(U_{se,d} - U_{se} + \rho(U_{se,p} - U_{se,d})). \tag{7}$$

Parameters $U_{se,d}$ and $U_{se,p}$ represent the depressed and potentiated states of the release probability U_{se}, and τ_{Use} is the time-constant of the presynaptic long-term plasticity.

Postsynaptic long-term plasticity corresponds to an insertion/removal of glutamatergic AMPAR,

$$\frac{dC_{AMPA}}{dt} = \frac{1}{\tau_{C_{AMPA}}}(C_{AMPA,d} - C_{AMPA} + \rho(C_{AMPA,p} - C_{AMPA,d})). \quad (8)$$

Parameters $C_{AMPA,d}$ and $C_{AMPA,p}$ represent the depressed and potentiated states of the AMPAergic coupling strength $C_{AMPA}(t)$, and $\tau_{C_{AMPA}}$ is the time-constant of the postsynaptic long-term plasticity. For simplicity, we assume that presynaptic and postsynaptic long-term changes have the same timescales $\tau_{Use} = \tau_{C_{AMPA}}$.

Whole model of pre- and postsynaptic plasticity reads as follows:

$$\frac{dr}{dt} = \frac{1-r}{\tau_r} - u\, r\, FR_{pre}\,, \quad (9a)$$

$$\frac{du}{dt} = \frac{U_{se}-u}{\tau_f} + U_{se}(1-u)FR_{pre}, \quad (9b)$$

$$\frac{d[Ca]}{dt} = I_{NMDA}^{[Ca]} - \frac{[Ca]}{\tau_{ca}}, \quad (9c)$$

$$\frac{d\rho}{dt} = \frac{1}{\tau_\rho}(-\rho(1-\rho)(\rho_* - \rho) + (1-\rho)\Omega_p([Ca]) - \rho\Omega_d([Ca])), \quad (9d)$$

$$\frac{dU_{se}}{dt} = \frac{1}{\tau_{Use}}\Big(U_{se,d} - U_{se} + \rho\big(U_{se,p} - U_{se,d}\big)\Big), \quad (9e)$$

$$\frac{dC_{AMPA}}{dt} = \frac{1}{\tau_{C_{AMPA}}}(C_{AMPA,d} - C_{AMPA} + \rho(C_{AMPA,p} - C_{AMPA,d})). \quad (9f)$$

Table 1: Parameters of (9) and their values unless otherwise stated

θ_d	depression threshold	0.1
θ_p	potentiation threshold	0.4
γ_d	depression amplitude	1

γ_p	potentiation amplitude	5
β_d	depression slope	80
β_p	potentiation slope	80
μ	slope of NMDA-dependent postsynaptic depolarization	1
V_{th}	threshold of NMDA-dependent postsynaptic depolarization	5 V
h_{Ca}	calcium current scaling factor	10
τ_d	presynaptic short-term depression time constant	0.200 sec
τ_f	presynaptic short-term facilitation time constant	0.05 sec
τ_{Ca}	the calcium influx decay time constant	0.05 sec
τ_ρ	synaptic efficacy time constant	50 sec
τ_{Use}	presynaptic long-term plasticity time constant	100 sec
$\tau_{C_{AMPA}}$	postsynaptic long-term plasticity time constant	100 sec
$U_{se,d}$	Value of depressed release probability	0.4
$U_{se,p}$	Value of potentiated release probability	0.8
$C_{AMPA,d}$	Value of depressed AMPAergic coupling strength	50
$C_{AMPA,p}$	Value of potentiated AMPAergic coupling strength	100

The revisited neural mass model

We revisited a minimal NMM of the CA1 region of the hippocampus [40] for obtaining an autonomous model that can undergoes seizures for a fixed parameter set. The original model includes four interacting neuronal subpopulations: two interconnected subpopulations of glutamatergic pyramidal neurons (P, P'), and two subpopulations of GABAergic inhibitory interneurons (somatostatin positive (SOM+), and parvalbunim positive (PV+), also called dendrite-projecting slow and soma-projecting fast interneurons, respectively). The activity of each subpopulation is described by a ``wave to pulse'' function, $S(v) = 5/(1 + exp(0.56(6 - v)))$, transforming the net membrane polarization in response to synaptic inputs

into a firing rate. The synaptic interactions between the subpopulations is described by a ``pulse to wave'' that converts the input average firing rate into a postsynaptic potential (PSP), which can be either excitatory – EPSP - or inhibitory - IPSP) at the input of each subpopulation, that is $h(t) = W/\tau_w\ t\ exp(-t/\tau_w)$, where W represents the average PSP amplitude. The equations of an unconnected population i POP_i reads:

$$\frac{d^2 y_P^{(i)}}{dt^2} = \frac{A^{(i)}}{\tau_a} S[V_P^{(i)}] - \frac{2}{\tau_a}\frac{dy_P^{(i)}}{dt} - \frac{1}{\tau_a^2}\, y_p^{(i)}, \quad (10a)$$

$$\frac{d^2 y_{P'}^{(i)}}{dt^2} = \frac{A^{(i)}}{\tau_a}(p(t) + C_{P',P}^{(i)}\, S\left[C_{P,P'}^{(i)} y_P^{(i)}\right]) - \frac{2}{\tau_a}\frac{dy_{P'}^{(i)}}{dt} - \frac{1}{\tau_a^2}\, y_{P'}^{(i)}, \quad (10b)$$

$$\frac{d^2 y_{SOM}^{(i)}}{dt^2} = \frac{B^{(i)}}{\tau_b}\, S[C_{P,SOM}^{(i)} y_P^{(i)}] - \frac{2}{\tau_b}\frac{dy_{SOM}^{(i)}}{dt} - \frac{1}{\tau_b^2}\, y_{SOM}^{(i)}, \quad (10c)$$

$$\frac{d^2 y_{PV}^{(i)}}{dt^2} = \frac{G^{(i)}}{\tau_g}\, S[C_{P,PV}^{(i)} y_P^{(i)} - C_{SOM,PV}^{(i)} y_{SOM}^{(i)}] - \frac{2}{\tau_g}\frac{dy_{PV}^{(i)}}{dt} - \frac{1}{\tau_g^2}\, y_{PV}^{(i)}, \quad (10d)$$

Parameters $C_{k,p}^{(i)}$ scales the impact from subpopulation k to subpopulation p within the population POP_i. The net polarization of P subpopulation of POP_i, $V_P^{(i)}$, reads,

$$V_P^{(1)} = \Sigma(C_{k,P}^{(1)}\, y_k^{(1)})$$

for POP_1, and,

$$V_P^{(2)} = \Sigma\left(C_{k,P}^{(2)}\, y_k^{(2)}\right) + \Sigma Input_{POP_1 \to POP_2}$$

for POP_2, which is subject to the excitatory AMRAergic and NMDAergic signals from POP_1 on its P subpopulation, $\Sigma Input_{POP_1 \to POP_2}$. We consider $V_P^{(i)}$ as the model output, which is a simplified proxy for the local field potential recorded by an extracelluar electrode positioned in the neuronal population.

Intracranial recordings from epileptic patients with focal epilepsy show four distinct phases of activity: interictal phase with sporadic spikes, preictal phase with periodic preictal spikes, low-voltage fast onset marked by a gamma-band activity, and tonic discharges [42]. Recordings show sequential transitions

between these phases, that is, interictal, preictal, then, ictal phase (so-called *seizure*, which starts with a tonic low-voltage fast onset phase followed by clonic discharges). For an appropriate choice of model parameters, the transitions between these phases in (10) can be obtained by varying the IPSP amplitude of the SOM interneurons, $\mathrm{B}^{(\mathrm{i})}$, (e.g. [40,43]). Figure 2A shows the bifurcation diagram of (10) for POP_1 as a function of $B^{(1)}$ with the parameter set in Table 2. The branch of equilibrium points undergoes four Hopf bifurcations at $B^{(1)} \approx \{0.47, 2.66, 9.98, 32.14\}$ and saddle-node bifurcations at $B^{(1)} \approx \{2.60, 2.92, 32.01, 50.38\}$. The gamma-band oscillations lie in $B^{(1)} \approx (2.66, 0.47)$ and the tonic lower frequency oscillations in $B^{(1)} \approx (9.98, 32.14)$. Under a stochastic input, such as $\mathrm{p(t)} = \mathcal{N}(p_m, p_S)$ in (10b), the gamma-band oscillations can be observed for $0 < B^{(1)} < 4$, the tonic phase for $4 < B^{(1)} < 32$. The low-frequency periodic preictal spikes and aperiodic interictal spikes can be located at the boundary between tonic oscillations and stable equilibrium points for $32 < B^{(1)} < 50$.

Figure 2 Dynamics of (10)-(11) in the interictal and ictal regimes. (A-D) Dynamics of (10)-(11) in the interictal regime for $b_{thr}^{(1)} = 34$. (A) Bifurcation diagram of (10) where the amplitude of $y_P^{(1)}$ is presented as a function of $B^{(1)}$. The blue curve shows the branch of equilibrium points (bold for stable and dashed for unstable equilibrium points). The red curves show the amplitude of $y_P^{(1)}$ in the oscillatory regime. The Hopf bifurcations along the branch of equilibrium points are denoted by red dots and saddle-node bifurcation by blue dots. The parameter regions correspond to the fast onset, ictal and interictal periods are marked by purple, yellow and cyan patches, respectively. The time solution (black curve) is superimposed on the bifurcation diagram. (B) Time trace for $V_P^{(1)}$ showing interictal spikes. (C) Phase plane of (11) with the $B^{(1)}$-nullcline (blue curve, bold for stable and dashed for branches) and the $n^{(1)}$-nullcline (orange curve). The parameter regions correspond to the fast onset, ictal and interictal periods are marked by green, yellow and cyan patches, respectively. The time solution (black curve) is superimposed on the bifurcation diagram. (D) Time trace for $B^{(1)}$. (E-H) Dynamics of (10)-(11) in the ictal regime for $b_{thr}^{(1)} = 32$. Same color codes and markers in (A-D) is used. Arrows in panel (G) indicates the direction of the trajectory (black curve) on the $(B^{(1)}, n^{(1)})$-plane with double arrows indicating the fast

transitions. The fast onset, ictal and interictal periods are marked on the time traces of $V_P^{(1)}$ and $B^{(1)}$ on panels F and H, respectively.

One can ensure an autonomous transition between the phases of epileptic activity by modeling $\mathrm{B}^{(\mathrm{i})}$ as a variable that varies in the range where they are observed. Here, we introduce a slow-subsystem where the IPSP amplitude of the SOM interneurons $B^{(i)}$ is a variable:

$$\frac{dB^{(i)}}{dt} = \delta\left(n^{(i)} - \left(-\frac{m_1\left(B^{(i)}-p_1\right)^2}{1+exp(-p_1+B^{(i)})} + \frac{1}{1+exp(-p_2+B^{(i)})} + \frac{m_3\left(B^{(i)}-p_3\right)^2}{1+exp(-p_3+B^{(i)})}\right)\right), \tag{11a}$$

$$\frac{dn^{(i)}}{dt} = \varepsilon\left(-n^{(i)} + n_k + \frac{n_p}{1+\exp\left(-n_r\left(b_{thr}^{(i)} - B^{(i)}\right)\right)}\right). \tag{11b}$$

Parameters of the $B^{(i)}$- and $n^{(i)}$-nullclines can be adjusted with respect to the critical (bifurcation) points of (10), desired type and range of behavior. Parameters of (11) are given in Table 2. In this study, the parameter $b_{thr}^{(i)}$ is the main parameter controlling the excitability, hence, the susceptibility of seizing of $\mathrm{POP_i}$.

Table 2: Parameters values for (10)-(15) unless otherwise stated

	Parameters of (10)	$\mathrm{POP_1}$	$\mathrm{POP_2}$
$A^{(i)}$	EPSP amplitude [mV]	5	5
$B^{(i)}$	$\mathrm{IPSP_{SOM}}$ amplitude [mV]	Variable	
$G^{(i)}$	$\mathrm{IPSP_{PV}}$ amplitude [mV]	20	2

τ_a	EPSP time constant [s]	0.01	0.01
τ_b	$IPSP_{SOM}$ time constant [s]	0.03	0.03
τ_g	$IPSP_{PV}$ time constant [s]	0.003	0.003
$C^{(i)}_{P,P'}$	$P \rightarrow P'$ coupling coefficient	135	135
$C^{(i)}_{P',P}$	$P' \rightarrow P$ coupling coefficient	108	108
$C^{(i)}_{SOM,P}$	$SOM \rightarrow P$ coupling coefficient	35	35
$C^{(i)}_{PV,P}$	$PV \rightarrow P$ coupling coefficient	200	200
$C^{(i)}_{P,SOM}$	$P \rightarrow SOM$ coupling coefficient	25	25
$C^{(i)}_{P,PV}$	$P \rightarrow PV$ coupling coefficient	200	200
$C^{(i)}_{SOM,PV}$	$SOM \rightarrow PV$ coupling coefficient	120	120
	Parameters of (11)		
p_1	local maximum of the $B^{(i)}$-nullcline	25	25
p_2	inflection point of the middle branch of the $B^{(i)}$-nullcline	30	30
p_3	local minimum of the $B^{(i)}$-nullcline	33	33
m_1	slope of the of the left branch of $B^{(i)}$-nullcline	0.0015	0.0015
m_3	slope of the of the right branch of the $B^{(i)}$ −nullcline	0.003	0.003
n_k	minimum of the n-nullcline	-0.2	-0.2
n_p	maximum of the n-nullcline sigmoid	1.4	1.4
n_r	slope of the n-nullcline at the inflection point	2	2
$b^{(i)}_{thr}$	inflection point of the n-nullcline	34	44
δ	time-scale parameter	50	50
ε	time-scale parameter	0.05	0.05
	Parameter values of (12)-(15)		
$A^{(2)}_{AMPA}$	AMPAergic-EPSP amplitude [mV]	-	10

$A_{NMDA}^{(2)}$	NMDAergic-EPSP amplitude [mV]	-	2
$A_{NMDA,ext}^{(2)}$	Extrasynaptic NMDAergic-EPSP amplitude [mV]	-	1
τ_{AMPA}	AMPAergic-EPSP time constant [s]	-	0.005
τ_{NMDA}	NMDAergic-EPSP time constant [s]	-	0.02
$\tau_{NMDA,ext}$	Extrasynaptic NMDAergic-EPSP time constant [s]	-	0.04
C_{NMDA}	NMDAergic coupling coefficient	-	$C_{AMPA,min}$
τ_K	Extrasynaptic NMDA integration time constant	-	10

Note that the system (11) is a slow-fast system itself, where $B^{(i)}$ is the fast and $n^{(i)}$ is the slow variable. The $B^{(i)}$-nullcline of (11) has an N-shape with stable outer and unstable middle branches (Fig 3C). System (10) governs the interictal and preictal phases for the $B^{(i)}$ values on the right branch $B^{(i)}$-nullcline. The $B^{(i)}$ values on the left and middle branches $B^{(i)}$-nullcline correspond to the ictal phase (fast-onset and tonic discharges) of (10). Depending on the position of the equilibrium point of (11), defined as the intersection between the N-shaped $B^{(i)}$-nullcline and sigmoidal $n^{(i)}$-nullcline, the system (11) follows either a steady state or an oscillatory solution. If the equilibrium point is close to the right fold point of the $B^{(i)}$-nullcline, then (11) is in an excitable state. If the equilibrium point is at the right handside of the right fold, any perturbation on $B^{(i)}$ can trigger a jump to the left branch of the fast nullcline, which corresponds to the ictal regime starting with the fast-onset activity. As the trajectory of (11) moves along the left branch of the $B^{(i)}$-nullcline, the system (10) undergoes the fast-onset, then tonic spiking before jumping back to the right branch, that is the interictal regime.

Modeling plasticity with coupled neural mass models

We consider two populations POP_1 and POP_2 modelled by the NMM formulation given in (10)-(11). POP_2 receives excitatory inputs from POP_1 through AMPAergic and NMDAergic signaling. Let $FR_P^{(1)}$ be the

firing rate of the P subpopulation of the POP_1, $r^{(1)}(t)$ and $u^{(1)}(t)$ are the variables describing the presynaptic neurotransmitter release (6). Then the AMPAergic excitatory PSP (EPSP) is the solution of

$$\frac{d^2 y_{AMPA}}{d^2 t} = \frac{r^{(1)} u^{(1)} A^{(2)}_{AMPA}}{\tau_{AMPA}} FR_P^{(1)} - \frac{2}{\tau_{AMPA}} \frac{dy_{AMPA}}{dt} - \frac{1}{\tau^2_{AMPA}} y_{AMPA}, \quad (12)$$

where τ_{AMPA} is the synaptic time constant and $A^{(2)}_{AMPA}$ is the amplitude that is modulated by STP variables, $r^{(1)}(t)$ and $u^{(1)}(t)$. The NMDAergic-EPSP is the solution of

$$\frac{d^2 y_{NMDA}}{d^2 t} = \frac{r^{(1)} u^{(1)} A^{(2)}_{NMDA}}{\tau_{NMDA}} FR_P^{(1)} - \frac{2}{\tau_{NMDA}} \frac{dy_{NMDA}}{dt} - \frac{1}{\tau^2_{NMDA}} y_{NMDA}, \quad (13)$$

where τ_{NMDA} is the synaptic time constant and $A^{(2)}_{NMDA}$is the amplitude. The NMDAergic EPSP are slower than the AMPAergic EPSP [44], thus $\tau_{AMPA} < \tau_{NMDA}$. The net depolarization of the postsynaptic subpopulation due to the activation of NMDAR depends on the postsynaptic potential, V_P^2 as well as the presynaptic entry $C_{NMDA} y_{NMDA}$, i.e. $C_{NMDA} y_{NMDA} H(V_P^2)$, with C_{NMDA} is the coupling strength.

The pathological plasticity is activated when both the probability of vesicle opening U_{se} and the AMPAR insertion C_{AMPA} are potentiated (9). Under this condition, an afferent epileptic spike from POP_1, which releases high levels of glutamate, activates the extrasynaptic NMDAR. The EPSP mediated by extrasynaptic NMDR, $y_{NMDA,ext}$, has slower kinetics then the EPSP mediated by synaptic NMDAR [45] (i.e. $\tau_{NMDA} < \tau_{NMDA,ext}$) and $y_{NMDA,ext}$is the solution of the following equation

$$\frac{d^2 y_{NMDA,ext}}{d^2 t} = \frac{r^{(1)} u^{(1)} A^{(2)}_{NMDA,ext}}{\tau_{NMDA,ext}} FR_P^{(1)} - \frac{2}{\tau_{NMDA,ext}} \frac{dy_{NMDA,ext}}{dt} - \frac{1}{\tau^2_{NMDA,ext}} y_{NMDA,ext}, \quad (14)$$

with the postsynaptic depolarization $C_{NMDA} y_{NMDA,ext} H(V_P^2)$, . The net postsynaptic polarization the P subpopulation of the POP_2 then reads,

$$V_P^{(2)} = \Sigma\left(C^{(2)}_{k,P}\, y_k^{(2)}\right) + C_{AMPA} y_{AMPA} + C_{NMDA}(y_{NMDA} H(V_P^2) + y_{NMDA,ext} H(V_P^2))$$

with the plastic $C_{AMPA}(t)$ given in (12) and constant C_{NMDA}.

The changes in GABAergic activity caused by the activation of extrasynaptic NMDAR is modeled via an auxiliary variable $K(t)$,

$$\frac{dK}{dt} = \frac{1}{\tau_K}\left(-K(0.5-K)(1-K) - C_{NMDA}y_{NMDA,ext}H\left(V_P^{(2)}\right)\right). \quad (15)$$

When extrasynaptic NMDAR is inactive (i.e. $y_{NMDA,ext} = 0$, (14) has three equilibrium points at $K^* = \{0, 0.5, 1\}$. The extrasynaptic NMDAR activation (i.e. $y_{NMDA,ext} \neq 0$) can lead to a saddle-node bifurcation of the equilibria $K^* = 0.5$ and $K^* = 1$ leaving (15) with a single equilibrium point at $K^* \approx 0$. The variable $K(t)$ modulates the excitability of POP_2 as,

$$b_{thr}^{(2)}(t) = b_{thr}^{(2)} - k_B^{(2)}(1 - K(t)),$$

where the parameter $k_B^{(2)}$ scales the impact of $K(t)$ on the excitability. Since the gamma-band activity observed at the seizure onset can be obtained by increasing the IPSP amplitude of PV interneurons [40,43], $K(t)$ modulates $G^{(2)}$ as

$$G^{(2)}(t) = G^{(2)} + k_G^{(2)}(1 - K(t)),$$

where the parameter $k_G^{(2)}$ scales the impact of $K(t)$ on the IPSP amplitude. We assumed that, in the absence of extrasynaptic NMDAR activity, $K(t) = 1$, for which IPSP amplitude is too small for yielding a gamma-band activity in (10)and the equilibrium point of (11) is far from the critical point of the seizure transition (i.e. the $n^{(2)}$-nullcline intersects the $B^{(2)}$-nullcline on its right branch). As $K(t) \to 0$ with the activation of the extrasynaptic NMDAR, $G^{(2)}(t)$ increases to a suitable level for obtaining gamma-band activity, whereas $b_{thr}^{(2)}(t)$ decreases and drives the equilibrium point of (10) towards the critical point of seizure transition in (10)-(11). In other words, how far (11) is from a Hopf bifurcation, hence how far (10) is from seizing, is controlled by the extrasynaptic NMDAR activity.

The parameter values of equations (10)-(15) are given in Table 2. Stochastic differential equations were iterated using Euler-Maruyama method with a step size dt = 10−5 second. Bifurcation analysis was done with AUTO-07p [46].

Results

Physiological plasticity

The model of physiological plasticity includes presynaptic STP, calcium-driven pre- and postsynaptic LTP/LTD and consolidation (Eq (9), Figure 1A). All these mechanisms have distinct timescales, and therefore the system describing the physiological plasticity (9) is a multiple timescale system with $(\tau_d, \tau_f) < \tau_{Ca} < \tau_\rho < \tau_{Use} = \tau_{C_{AMPA}}$. We assume that the slow regime is governed by the variables concerning LTP/LTP and consolidation, e.g. (ρ, U_{se}, C_{AMPA}). In the slow regime, the fast variables describing STP, $r^{(1)}$ and $u^{(1)}$, are slaved to the slow variables, as:

$$r^{(1)s} = \frac{1}{1 + \tau_d \, u^{(1)s} \, FR_P^{(1)}}, \qquad u^{(1)s} = \frac{U_{se}(1 + \tau_f FR_P^{(1)})}{1 + \tau_f U_{se} \, FR_P^{(1)}}$$

where superscript $(.)^s$ indicates the slow regime. The NMDA-mediated calcium dynamics in the slow regime is given by

$$[Ca]^s = \tau_{Ca} \, G\left(FR_P^{(1)}\right) h_{Ca} H(V_P^2) = \tau_{Ca} \, C_{NMDA} \, y_{NMDA}(t) h_{Ca} H(V_P^2).$$

The NMDAergic-EPSPs $y_{NMDA}(t)$ can be approximated by $y_{NMDA} \approx \tau_{NMDA} \, A_{NMDA}^{(2)} \, r^{(1)s} \, u^{(1)s} \, FR_P^{(1)}$. If similar is applied for the AMPAergic synapses, $y_{AMPA} \approx \tau_{AMPA} \, A_{AMPA}^{(2)} \, r^{(1)s} \, u^{(1)s} \, FR_P^{(1)}$, then postsynaptic potential $V_P^{(2)}$ is given by

$$V_P^{(2)} = \Sigma\left(C_{k,P}^{(2)} \, y_k^{(2)}\right) + C_{AMPA} \tau_{AMPA} \, A_{AMPA}^{(2)} \, r^{(1)s} \, u^{(1)s} \, FR_P^{(1)} + C_{NMDA} \tau_{NMDA} \, A_{NMDA}^{(2)} \, r^{(1)s} \, u^{(1)s} \, FR_P^{(1)}.$$

For the NMDA-mediated calcium entry and postsynaptic depolarization to occur, the postsynaptic membrane should be sufficiently depolarized, i.e. $V_P^{(2)} > V_{th}$. This depolarization depends on the AMPAergic input. Assuming that the postsynaptic system is balanced for $FR_P^{(1)} = 0$ and intra-population interactions are independent of the external input, i.e. $\Sigma\left(C_{k,P}^{(2)} \, y_k^{(2)}\right) = 0$, the postsynaptic polarization in response to the AMPAergic input from POP_1 can be reduced to

$$V_P^{(2)} \approx C_{AMPA}\tau_{AMPA}\, A_{AMPA}^{(2)}\, r^{(1)s}\, u^{(1)s}\, FR_P^{(1)},$$

calcium concentration to

$$[Ca]^s = C_{NMDA}\tau_{NMDA}\, A_{NMDA}^{(2)}\, r^{(1)s}\, u^{(1)s}\, FR_P^{(1)} h_{Ca}, \text{if } V_P^{(2)} > V_{th}, \text{otherwise } [Ca]^s \approx 0$$

As the fast variables $(r^{(1)}, u^{(1)}, [Ca])$ are expressed as a function of the slow variables, (ρ, U_{se}, C_{AMPA}), the reduced (slow) system reads:

$$\frac{d\rho}{d\,\bar{t}} = (-\rho(1-\rho)(\rho_* - \rho) + (1-\rho)\Omega_p([Ca]) - \rho\Omega_d([Ca])), \tag{16a}$$

$$\frac{dU_{se}}{d\bar{t}} = \frac{\tau_\rho}{\tau_{Use}}(U_{se,d} - U_{se} + \rho(U_{se,p} - U_{se,d})). \tag{16b}$$

$$\frac{dC_{AMPA}}{d\bar{t}} = \frac{\tau_\rho}{\tau_{C_{AMPA}}}(C_{AMPA,d} - C_{AMPA} + \rho(C_{AMPA,p} - C_{AMPA,d})). \tag{16c}$$

where $\bar{t} = \frac{t}{\tau_\rho}$. If $\frac{\tau_\rho}{\tau_{Use}} = \frac{\tau_\rho}{\tau_{C_{AMPA}}} \ll 1$, then we can take them to zero limit and thread them as parameters to investigate the variation of ρ under plasticity, which is the variable that controls the long-term variations in the neurotransmitter release probability, U_{se}, and the AMPARergic coupling strength, C_{AMPA}. For a simple investigation of ρ (16a) for $\frac{\tau_\rho}{\tau_{Use}} = \frac{\tau_\rho}{\tau_{C_{AMPA}}} = 0$, we assume that $C_{AMPA} \approx C_{AMPA,min} + \kappa\, U_{se}$, $(\kappa > 0)$, which is a reasonable assumption since both C_{AMPA} and U_{se} depend on ρ in the same manner. Figure 4(A) and (B) shows $V_P^{(2)}$ and $[Ca]^s$ as a function of $FR_P^{(1)}$ and U_{se} with the parameter set given in Table 1. The postsynaptic subpopulation depolarizes monotonically for increasing $FR_P^{(1)}$ and U_{se} (Fig 4(A)). The change in the calcium concentration follows a sigmoidal shape (Fig 4(B)). It remains close to zero for low values of U_{se} and $FR_P^{(1)}$. It increases sharply for medium values of U_{se} and $FR_P^{(1)}$, then slowly for higher values of $U_{se}$and $FR_P^{(1)}$ as it approaches a plateau.

Figure 3 Physiological plasticity at presynaptic and postsynaptic sites. (A) Presynaptic glutamatergic release and subsequent postsynaptic depolarization results in calcium influx via NMDARs. Calcium signaling activates independent biochemical pathways, leading to postsynaptic and presynaptic long-term changes due to the insertion of new AMPARs and an increase in vesicle release probability. Under

physiological conditions, excitation is balanced by sufficient chloride trafficking through GABAR and KCC2. (B) Pathological plasticity at postsynaptic site. When the released glutamate is too high to be used by synaptic AMPAR and NMDAR, it diffuses to the extrasynaptic site and activates the extrasynaptic NMDAR. Activation of NMDAR causes internalization of extrasynaptic GABAR. Calcium influx via the extrasynaptic NMDAR activates calpain that perturbs the KCC2 functioning.

Figure 4 Postsynaptic depolarization, calcium concentrating and long-term plasticity in sow regime. (A) Postsynaptic polarization $V_P^{(2)s}$ and (B) calcium concentration $[Ca]^s$ as a function of $\left(FR_P^{(1)}, U_{se}\right)$ for the parameter set given in Table 1 and $\gamma_p = 1$. (C) Equilibrium points of (16a) as function of $\left(FR_P^{(1)}, U_{se}\right)$ for different values of (θ_p, θ_d).

We then investigate the variation of ρ under plasticity. For this, we compute the equilibrium points of (16) for $\frac{dU_{\{se\}}}{d\bar{t}} = \frac{dC_{AMPA}}{d\bar{t}} = 0$. In particular, (16a) has three equilibrium points at $\rho^* = \{0, 0.5, 1\}$ if the variations in U_{se} and $FR_P^{(1)}$ are not sufficient to change, meaning that depressed synapses will remain depressed, and the potentiated ones will remain potentiated. If U_{se} and $FR_P^{(1)}$ are in a region where they can induce any change in ρ , (16a) has a single stable equilibrium point. If $\rho^* \in [0, 0.5)$ then the synapses will depress, if $\rho^* \in (0.5, 1]$ then the synapses will potentiate. Figure 4(C) shows ρ^* as a function of $(FR_P^{(1)}, U_{se})$ as the LTD and LTP thresholds, θ_d and θ_p, vary on this calcium concentration surface. The dark blue regions indicate that (16a) has three equilibrium points at $\rho^* = \{0, 0.5, 1\}$, therefore, the synapses do not change. When the potentiation threshold θ_p is too high ($\theta_p = 1.5$, upper panels), synapses either do not change or become depressed for moderate to high input firing rates $FR_P^{(1)}$ and release probability U_{se} depending on the depression threshold θ_d. A decreasing difference between θ_d and θ_p widens the $(FR_P^{(1)}, U_{se})$ region for which (16a) has three equilibria. Consequently, both synapses preserve their values for a low presynaptic firing rate. Lowering the potentiation threshold expands the range of LTP. In this case, increasing θ_d shrinks the LTD range.

Physiological plasticity under epileptic activity

In our model, long-term plasticity depends on the time lag between the interictal spikes of POP_1 and POP_2, as well. In this section we assume that only the physiological synaptic plasticity mechanism (Fig 1A) is active. Figure 5 exemplifies how ρ changes in response to single spikes of POP_1 and POP_2 elicited by a pulse stimulation when ρ is initiated at $\rho(0) = 0.5$. The synaptic variable ρ potentiates regardless of the pulse delay for $(\theta_d, \theta_p) = (0.6, 0.7)$, depresses $(\theta_d, \theta_p) = (0.1, 0.7)$ (Fig 5A). We obtain a depression-potentiation-depression curve of $\Delta\rho$ for $(\theta_d, \theta_p) = (0.3, 0.7)$, for which the system response is shown in Figure 5B-D. When POP_2 spikes $\Delta t = 0.02\ sec$ before POP_1, the calcium concentration stays between (θ_d, θ_p) and ρ decreases (Fig 5B). When POP_2 and POP_1 spike simultaneously, the calcium concentration exceeds θ_p and ρ increases (Fig 5C). Finally, when POP_2 spikes $\Delta t = 0.02\ sec$ after POP_1, ρ decreases since the calcium concentration stays between (θ_d, θ_p) (Fig 5D).

Figure 5 Change in synaptic efficacy under epileptic spikes. (A) Rate of change in the synaptic efficacy variable ρ under single epileptic spike in in Pop1 and Pop2 when the system (9)-(10) is initialized from $\rho(0) = 0.5$ with $(U_{se}, C_{AMPA}) = (U_{se,min}, C_{AMPA,min})$. Epileptic spikes are triggered by a pulse stimulation applied with a time delay of Δt (sec) for $(\theta_d, \theta_p) = (0.1, 0.7)$ (green line), $(\theta_d, \theta_p) = (0.3, 0.7)$ (orange line) and $(\theta_d, \theta_p) = (0.1, 0.7)$ (blue line) . (B-D) Pre- and post-spiking is triggered by a single pulse with $\Delta t = -0.2\ sec$ in (B), $ $\Delta t = 0$ in (C) and $\Delta t = 0.2$ in (D) for $(\theta_d, \theta_p) = (0.3, 0.7)$. The corresponding behaviour of $[Ca]$ and ρ are shown in the middle and bottom panels, respectively. The orange dotted and green dotted lines in the middle panels mark θ_d and θ_p, respectively.

Depending on the potentiation and depression thresholds, and intrinsic dynamics of the interacting populations, aperiodic but continuous interictal epileptic discharges can cause long-term changes in the presynaptic release probability and coupling strength between the interacting populations (Fig 6). Here, we assume that POP_1 is in interictal spiking mode as in Fig 2B, and the less excitable POP_2 responds to POP_1 by generating spikes. If the potentiation threshold is high, then initially depressed synapses between POP_1 and POP_2 remain depressed (Fig 6A). For a lower potentiation threshold, the

depolarization in POP_2 is high enough to increase the calcium concentration above θ_p, hence causing a positive change in the synaptic variable ρ ($\Delta\rho > 0$). If this regime is maintained long enough and (θ_d, θ_p) are in a suitable range for LTP, ρ can cross the threshold separating depressed to potentiated states, and a pre- and postsynaptic LTP occurs (Fig 6B). Because of the LTP, the time lag between the POP_1 and POP_2 spikes decreases. In the same configuration but with potentiated synapses, increasing the difference between θ_d and θ_p causes pre- and postsynaptic LTD since the calcium concentration remains in (θ_d, θ_p) (Fig 6C). Consequently, the time lag between the POP_1 and POP_2 spikes increases. If both depression and potentiation thresholds are high, despite the interaction between POP_1 and POP_2, synaptic variables do not change (Fig 6D).

Figure 6 Physiological plasticity under inter-ictal epileptic discharges. (A) No change in depressed synapses for $(\theta_d, \theta_p) = (0.3, 0.7)$. (B) Potentiation of initially depressed synapses for $(\theta_d, \theta_p) = (0.3, 0.4)$. (C) Depression of initially potentiated synapses for $(\theta_d, \theta_p) = (0.1, 1.5)$ (D) No change in potentiated synapses for $(\theta_d, \theta_p) = (1.2, 1.5)$.

Experimental studies suggest that high rate of synchronized activity, during an epileptic seizure for instance, increases the glutamate release. Indeed, the model also suggests that an increased firing rate during a seizure in POP_1 can drive the calcium concentration above θ_p, and cause LTP, while the interictal activity with the same values of (θ_d, θ_p) does not change synaptic efficacy (Fig. 6A vs 7A). Alternatively, if calcium concentration is already above θ_p, then the increased firing rate can accelerate LTP in POP_2 (Fig. 6B vs 7B). In Figure 7 the repeated seizures in POP_1 are triggered by a stochastic input to $B^{(1)}$ variable.

Figure 7 Impact of seizure to physiological plasticity. Potentiation of depressed synapses for $(\theta_d, \theta_p) = (0.3, 0.7)$ (A) and for $(\theta_d, \theta_p) = (0.3, 0.4)$ (B).

Expansion of the epileptogenic network

Physiological plasticity alone increases coupling strength by increasing the probability of neurotransmitter release at the presynaptic site and inserting AMPAR at the postsynaptic site. Unless the

extrasynaptic NMDAR are activated at the postsynaptic site, the postsynaptic population can preserve its excitation/inhibition balance, hence, does not undergo seizures. However, the extrasynaptic NMDAR activation triggers different processes that disturb the excitation/inhibition balance by reducing the effect of the GABARergic activity [7,47,48] (Fig 3B).

We assumed that the extrasynaptic NMDAR (14) is activated after the synapses are potentiated, i.e. for $U_{se} > 0.7$. The extrasynaptic NMDAR activity changes the amplitude of the PV INs $G^{(2)}(t)$ and the excitability $btr^{(2)}(t)$ of POP_2 via the auxiliary variable $K(t)$ (15). We investigate the impact of these changes in the whole model given by (9)-(15). We simulate the whole system (9)-(15) starting from the last point of the solution in Fig 7B for$(\theta_d, \theta_p) = (0.3, 0.4)$. When POP_1 undergoes seizures since low value of $btr^{(1)}$, and POP_2 responds by epileptic spikes since POP_2 has a low excitability because $btr^{(2)}(t)$ is initially high. Activation of the extrasynaptic NMDAR drives the variable $K(t)$ to 0 as it causes ``structural" changes within POP_2. In particular, the amount of the GABAergic loss in POP_2, which is represented by the parameter $k_B^{(2)}$, can decrease the excitablity threshold of POP_2 and cause seizures in POP_2. The relation between the GABAergic loss and seizure in POP_2 is represented in the phase space of $(B^{(2)}, n^{(2)})$ in Fig 8A, and the time traces are shown in Fig 8B. For $0 \leq k_B^{(2)} < 8$ the equilibrium point of the $(B^{(2)}, n^{(2)})$ −subsystem remains on the right handside of the critical point of the seizure transitions. In this regime, POP_2 responds to the seizures of POP_1 by spiking only, For $8 \leq k_B^{(2)}$, the variable $B^{(2)}$ crosses the critical point and jumps to the left branch of the $B^{(2)}$-nullcline, meanwhile POP_2 responds to the seizures of POP_1 with a seizure. POP_2 undergoes spontaneous and periodic seizures for $10 \leq k_B^{(2)}$.

Figure 8 Effect of the pathological plasticity on POP_2. (A) Phase portrait of $(B^{(2)}, n^{(2)})$-subsystem showing the effect of the parameter k_B on the excitability of POP_2. POP_2 crosses the critical point as k_B increases. (B) Time traces of $B^{(2)}$ shown in (A). (C) Normalized PSD of $V_P^{(2)}$ during seizures shows the effect of $k_G^{(2)}$ for $k_B = 9$. Gamma-band activity appears for $k_G^{(2)} > 8$. (D-E) Example time trace of (9)-(15)

for (E) $(k_B, k_G) = (0,0)$ and (F) $(k_B, k_G) = (9, 20)$. POP_2 undergoes a complete seizure in $t = (180, 230)$.

One of the markers of the seizure onset zone is the gamma-band activity observed at the seizure onset. Parameter $k_G^{(2)}$ scales the impact of the variable $K(t)$, hence of the activation of extrasynaptic NMDAR, on the fast GABAergic interneurons. POP_2 undergoes a gamma-band activity at the seizure onset for $k_G^{(2)} > 8$ as demonstrated in the power spectral density (PSD) of $V_P^{(2)}$ during a seizure triggered by POP_1 for $k_B^{(2)} = 9$ (Fig 8C). Figure 8E and F show the response of POP_2 for $\left(k_B^{(2)}, k_G^{(2)}\right) = (0, 0)$ and $\left(k_B^{(2)}, k_G^{(2)}\right) = (9, 20)$ for the epileptic spikes and seizure on POP_1, respectively. POP_2 undergoes a seizure at $t = (180, 230)$ after spiking as a response to a seizure in POP_1 at $t = (160, 190)$.

Resection of the epileptic zone

The activation of extrasynaptic NMDAR induces irreversible structural changes in POP_2, in particular, in its GABAergic structure. If the GABAergic loss is important, despite a completely silent POP_1, POP_2 continues to undergo epileptic activity. Figure 9 shows an example where at $t = 250\ sec$ POP_1 is silenced by setting $A^{(1)} = 0$ but POP_2 continues seizing.

Figure 9 Resection of the primarily focus. After the cessation of any form of activity in POP_1 at $t = 250$ (A), POP_2 continues to undergo spontaneous seizures (B).

Discussion

In this study, we presented a neurophysiologically plausible NMM of physiological and pathological plasticity under epileptic activity. Physiological plasticity takes into account short- and long-term variations in the glutamatergic interactions at both presynaptic and postsynaptic sites. Pathological plasticity considers GABARgic modulations at the postsynaptic site. Under epileptic activity, increased connectivity strength resulting from the physiological plasticity triggers the pathological plasticity, which

causes a secondary focus. These mechanisms have been implemented in an autonomous (self-driven) NMM, which generates the typical focal seizure pattern from interictal to seizure termination.

Physiological synaptic plasticity in the model integrates three main mechanisms. The first one is the presynaptic STP. The second one is the calcium-mediated long-term synaptic plasticity that changes the probability of glutamate release at the presynaptic site and insertion of AMPAR at the postsynaptic site. The third mechanism is the consolidation of long-term plasticity. Although the description of consolidation remained phenomenological as in [30,32], its integration into the model allowed for a sustained change in synaptic connectivity.

We assumed that presynaptic and postsynaptic long-term plasticity are proportional. While this simplified assumption is true for retrograde nitric oxide signaling, retrograde endocannabinoid release works in the opposite direction. Costa et al. [37] suggested a phenomenological model integrating the effects of opposing proteins on long-term presynaptic plasticity. Such effects can be integrated in our model, for instance, by introducing a second variable to track the calcium variations, which modifies the neurotransmitter release probability.

Our approach of modeling NMDA currents is quasi-physiological, similar to [38], but without explicitly modeling the magnesium gate. Yet, it does include the essential ingredients mediating the NMDAR activity, which are the presynaptic release and postsynaptic potentiation. Conductance-based modeling of synaptic receptors in the neural mass formulation has been proposed in [49], and more recently, in [50]. While the conductance-based neural mass formulation may provide a more physiological way of modeling neural dynamics, we argue that our approach is consistent with the neural mass formulation we considered and captures the key ingredients necessary for the problem studied.

The pathological plasticity under epileptic activity includes disruption of the GABAergic pathway caused by the activation of the extrasynaptic NMDAR. The model captures possible changes without detailing the process, such as how calcium entry through the extrasynaptic NMDAR acts on calpain, how a decreasing number of KCC2 changes the GABA reversal potential, or how GABAR expression is

downregulated, etc. Rather, the impact of the extrasynaptic NMDAR activation is reflected by an auxiliary variable that acts on perisomatic and dendritic GABAergic interneurons of the NMM. The former mimics the effect of KCC2 downregulation that induces a gamma-band activity, which is considered a signature of an epileptogenic zone in focal seizures. The latter mimics the effect of GABAR downregulation that reduces the excitability threshold of the population targeted by the epileptic population. Indeed, the dendritic SOM interneurons control the calcium dynamics, for instance by directly inhibiting calcium influx [51–53]. Low dendritic SOM projection may lead to accumulation of intracellular calcium and aggravate KCC2 dysfunctions.

In this study we extended a widely used model of the hippocampus [40] for ensuring autonomous epileptic activity from interictal to ictal and seizure termination. Essentially, this was achieved by introducing a slow subsystem that modulates the IPSP amplitude of the slow GABAergic interneurons. In other words, we introduced a basic slow-fast process for obtaining an autonomous interictal-to-ictal activity. Except for very few studies [54,55], the modulation has been performed manually to obtain ictal activity. In both studies, the main agent driving system to seizure is the IPSP amplitude of the slow GABAergic INs. In [55,56] a dynamic chloride accumulation in pyramidal neurons caused by GABAergic activity modulates the IPSP amplitude. However, the authors of [55] do not propose a mechanism for seizure termination. In [54] this modulation was obtained through feedback from the activity of the pyramidal cells. Our approach is similar to the phenomenological approach of [54], except the feedback from the pyramidal neurons and the dimension of the slow subsystem. In the transition to seizures, not only pyramidal neurons but also interneurons can play a critical role [57]. Our model can be improved further to reflect the involvement of specific cellular and network mechanisms by considering appropriate feedback mechanisms. Furthermore, the fast-system representing neuronal subpopulations and the slow-subsystem controlling the excitability and the IPSP amplitude have the essential ingredients for studying different bifurcation types, which can be inherent to specific seizure types (absence seizures, focal seizures with different seizure onset patterns [42]. Furthermore, the slow-fast system can be used

to study the effect of electrical stimulation that is a general procedure in clinics to understand the excitability of the brain region to identify epileptogenic networks.

Our study confirms the so-called *seizure can beget seizures* phenomena: epileptic activity in one brain region can recruit healthy regions and cause the formation of a complex epileptic network [58]. The model suggests that epileptic seizures boots physio-pathological plasticity, as suggested in the literature [8,59]. Once a healthy zone is driven to the critical point, then it generates epileptic discharges and/or seizures. Therefore, the timing of interference with epileptic activity may be critical. Indeed, in clinical practice, acute symptomatic seizures are treated with anti-seizure medication [60]. In addition to the role of epileptic activity in epileptogenesis, epileptic activity can interfere with physiological oscillatory activity in distributed neural networks and cause cognitive comorbidity [61–65]. Generalizing our model to personalized dynamic brain network modeling for planning the treatment of epilepsy is a future research direction [66].

On the other hand, epilepsy is a complex and patient-specific disease, and it is challenging to propose a "one-fits-all" theory. The "seizure beget seizure" phenomenon has been questioned recently [67], especially in the light of clinical data [68]. Our model has many limitations to address this challenge. First, it only considers glutamatergic plasticity mediated by epileptic activity between unidirectionally coupled neuronal populations. A growing body of literature suggests that inhibitory GABAergic synapses exhibit long-term plasticity, which can have a protective role against the expansion of epileptogenic networks [69,70]. The model does not address mGLUR mediated plasticity [71,72], homeostatic effects [73] or other mechanisms, such as epigenetic changes [74]. In addition, the considered NMM is the simplest formulation for the CA1 region of the hippocampus. A laminar NMM can be considered for the distant synaptic rules related to dendritic location, which can be useful for studying the plasticity induced in neocortical regions by non-invasive brain stimulation. Modeling experimental recording will be an asset. Finally, the model simulates epileptiform discharges, whereas the physiological plasticity is also mediated

by theta rhythm and theta-gamma oscillations in the hippocampus [75]. These points will be addressed in future works.

Conclusion

We have proposed a framework based on neural mass modeling for studying physio-pathological plasticity under epileptic activity. We have shown how increased connectivity between an epileptic and non-epileptic brain regions leads to GABAergic dysfunctions in the latter, and it forms an epileptogenic network. Our study can benefit the development of *plastic* large-scale brain models for studying the expansion of epileptogenic networks, formation of secondary foci, and the design of invasive or non-invasive brain stimulation protocols to control the epileptogenic networks.

Acknowledgement

This project has received funding from the European Research Council (ERC) under the European Union's Horizon 2020 research and innovation program (grant agreement No 855109).

References

1. Turrigiano GG, Nelson SB. Homeostatic plasticity in the developing nervous system. Nat Rev Neurosci. 2004 Feb;5(2):97–107.

2. Zhang W, Linden DJ. The other side of the engram: experience-driven changes in neuronal intrinsic excitability. Nat Rev Neurosci. 2003 Nov;4(11):885–900.

3. Abraham WC, Bear MF. Metaplasticity: the plasticity of synaptic plasticity. Trends Neurosci. 1996 Apr 1;19(4):126–30.

4. Scimemi A. Structure, function, and plasticity of GABA transporters. Front Cell Neurosci [Internet]. 2014 [cited 2023 Dec 12];8. Available from: https://www.frontiersin.org/articles/10.3389/fncel.2014.00161

5. Hennequin G, Agnes EJ, Vogels TP. Inhibitory Plasticity: Balance, Control, and Codependence. Annu Rev Neurosci. 2017;40(1):557–79.

6. Chiu CQ, Barberis A, Higley MJ. Preserving the balance: diverse forms of long-term GABAergic synaptic plasticity. Nat Rev Neurosci. 2019 May;20(5):272–81.

7. Khalilov I, Holmes GL, Ben-Ari Y. In vitro formation of a secondary epileptogenic mirror focus by interhippocampal propagation of seizures. Nat Neurosci. 2003 Oct;6(10):1079–85.

8. Ben-Ari Y. Epilepsies and neuronal plasticity: for better or for worse? Dialogues Clin Neurosci. 2008 Mar 31;10(1):17–27.

9. Ben-Ari Y, Holmes GL. Effects of seizures on developmental processes in the immature brain. Lancet Neurol. 2006 Dec 1;5(12):1055–63.

10. Citri A, Malenka RC. Synaptic Plasticity: Multiple Forms, Functions, and Mechanisms. Neuropsychopharmacology. 2008 Jan;33(1):18–41.

11. Zucker RS, Regehr WG. Short-Term Synaptic Plasticity. Annu Rev Physiol. 2002;64(1):355–405.

12. Malenka RC, Bear MF. LTP and LTD: An Embarrassment of Riches. Neuron. 2004 Sep 30;44(1):5–21.

13. Nevian T, Sakmann B. Spine Ca2+ Signaling in Spike-Timing-Dependent Plasticity. J Neurosci. 2006 Oct 25;26(43):11001–13.

14. Graupner M, Brunel N. Mechanisms of induction and maintenance of spike-timing dependent plasticity in biophysical synapse models. Front Comput Neurosci [Internet]. 2010 [cited 2022 May 18];4. Available from: https://www.frontiersin.org/article/10.3389/fncom.2010.00136

15. Schulz PE. Long-term potentiation involves increases in the probability of neurotransmitter release. Proc Natl Acad Sci. 1997 May 27;94(11):5888–93.

16. Yang Y, Calakos N. Presynaptic long-term plasticity. Front Synaptic Neurosci [Internet]. 2013 [cited 2023 Jan 24];5. Available from: https://www.frontiersin.org/articles/10.3389/fnsyn.2013.00008

17. Abegg MH, Savic N, Ehrengruber MU, McKinney RA, Gähwiler BH. Epileptiform activity in rat hippocampus strengthens excitatory synapses. J Physiol. 2004;554(2):439–48.

18. Goddard GV, Douglas RM. Does the Engram of Kindling Model the Engram of Normal Long Term Memory? Can J Neurol Sci J Can Sci Neurol. 1975 Nov;2(4):385–94.

19. Wu K, Castellano D, Tian Q, Lu W. Distinct regulation of tonic GABAergic inhibition by NMDA receptor subtypes. Cell Rep. 2021 Nov 9;37(6):109960.

20. Hardingham GE, Bading H. Synaptic versus extrasynaptic NMDA receptor signalling: implications for neurodegenerative disorders. Nat Rev Neurosci. 2010 Oct;11(10):682–96.

21. Lee HHC, Deeb TZ, Walker JA, Davies PA, Moss SJ. NMDA receptor activity downregulates KCC2 resulting in depolarizing GABAA receptor–mediated currents. Nat Neurosci. 2011 Jun;14(6):736–43.

22. Kahle KT, Deeb TZ, Puskarjov M, Silayeva L, Liang B, Kaila K, et al. Modulation of neuronal activity by phosphorylation of the K–Cl cotransporter KCC2. Trends Neurosci. 2013 Dec 1;36(12):726–37.

23. Kahle KT, Khanna AR, Duan J, Staley KJ, Delpire E, Poduri A. The KCC2 Cotransporter and Human Epilepsy: Getting Excited About Inhibition. The Neuroscientist. 2016 Dec 1;22(6):555–62.

24. Wu C, Sun D. GABA receptors in brain development, function, and injury. Metab Brain Dis. 2015 Apr;30(2):367–79.

25. Chen Q, He S, Hu XL, Yu J, Zhou Y, Zheng J, et al. Differential Roles of NR2A- and NR2B-Containing NMDA Receptors in Activity-Dependent Brain-Derived Neurotrophic Factor Gene Regulation and Limbic Epileptogenesis. J Neurosci. 2007 Jan 17;27(3):542–52.

26. Goldensohn ES. The Relevance of Secondary Epileptogenesis to the Treatment of Epilepsy: Kindling and the Mirror Focus. Epilepsia. 1984;25(s2):S156–68.

27. Shen Y, Gong Y, Ruan Y, Chen Z, Xu C. Secondary Epileptogenesis: Common to See, but Possible to Treat? Front Neurol [Internet]. 2021 [cited 2024 Jan 25];12. Available from: https://www.frontiersin.org/articles/10.3389/fneur.2021.747372

28. Kuang Y, Xu C, Zhang Y, Wang Y, Wu X, Wang Y, et al. Low-frequency stimulation of the primary focus retards positive transfer of secondary focus. Sci Rep. 2017 Mar 23;7(1):345.

29. Shouval HZ, Bear MF, Cooper LN. A unified model of NMDA receptor-dependent bidirectional synaptic plasticity. Proc Natl Acad Sci. 2002 Aug 6;99(16):10831–6.

30. Chindemi G, Abdellah M, Amsalem O, Benavides-Piccione R, Delattre V, Doron M, et al. A calcium-based plasticity model for predicting long-term potentiation and depression in the neocortex. Nat Commun. 2022 Jun 1;13(1):3038.

31. Kumar A, Mehta M. Frequency-Dependent Changes in NMDAR-Dependent Synaptic Plasticity. Front Comput Neurosci [Internet]. 2011 [cited 2022 May 18];5. Available from: https://www.frontiersin.org/article/10.3389/fncom.2011.00038

32. Graupner M, Brunel N. Calcium-based plasticity model explains sensitivity of synaptic changes to spike pattern, rate, and dendritic location. Proc Natl Acad Sci. 2012 Mar 6;109(10):3991–6.

33. Cai Y, Gavornik JP, Cooper LN, Yeung LC, Shouval HZ. Effect of Stochastic Synaptic and Dendritic Dynamics on Synaptic Plasticity in Visual Cortex and Hippocampus. J Neurophysiol. 2007 Jan;97(1):375–86.

34. Inglebert Y, Aljadeff J, Brunel N, Debanne D. Synaptic plasticity rules with physiological calcium levels. Proc Natl Acad Sci. 2020 Dec 29;117(52):33639–48.

35. Shouval HZ, Castellani GC, Blais BS, Yeung LC, Cooper LN. Converging evidence for a simplified biophysical model of synaptic plasticity. Biol Cybern. 2002 Dec 1;87(5):383–91.

36. Senn W, Markram H, Tsodyks M. An Algorithm for Modifying Neurotransmitter Release Probability Based on Pre- and Postsynaptic Spike Timing. Neural Comput. 2001 Jan 1;13(1):35–67.

37. Costa RP, Froemke RC, Sjöström PJ, van Rossum MC. Unified pre- and postsynaptic long-term plasticity enables reliable and flexible learning. Nelson SB, editor. eLife. 2015 Aug 26;4:e09457.

38. Fung PK, Robinson PA. Neural field theory of calcium dependent plasticity with applications to transcranial magnetic stimulation. J Theor Biol. 2013 May 7;324:72–83.

39. Modolo J, Thomas A, Legros A. Neural mass modeling of power-line magnetic fields effects on brain activity. Front Comput Neurosci [Internet]. 2013 [cited 2023 Feb 24];7. Available from: https://www.frontiersin.org/articles/10.3389/fncom.2013.00034

40. Wendling F, Bartolomei F, Bellanger JJ, Chauvel P. Epileptic fast activity can be explained by a model of impaired GABAergic dendritic inhibition. Eur J Neurosci. 2002;15(9):1499–508.

41. Tsodyks M, Pawelzik K, Markram H. Neural Networks with Dynamic Synapses. Neural Comput. 1998 May;10(4):821–35.

42. Lagarde S, Buzori S, Trebuchon A, Carron R, Scavarda D, Milh M, et al. The repertoire of seizure onset patterns in human focal epilepsies: Determinants and prognostic values. Epilepsia. 2019 Jan;60(1):85–95.

43. Köksal Ersöz E, Modolo J, Bartolomei F, Wendling F. Neural mass modeling of slow-fast dynamics of seizure initiation and abortion. PLOS Comput Biol. 2020 Nov 9;16(11):e1008430.

44. Zito K, Scheuss V. NMDA Receptor Function and Physiological Modulation. In: Squire LR, editor. Encyclopedia of Neuroscience [Internet]. Oxford: Academic Press; 2009 [cited 2023 Feb 3]. p. 1157–64. Available from: https://www.sciencedirect.com/science/article/pii/B9780080450469012250

45. Müller L, Tokay T, Porath K, Köhling R, Kirschstein T. Enhanced NMDA receptor-dependent LTP in the epileptic CA1 area via upregulation of NR2B. Neurobiol Dis. 2013 Jun 1;54:183–93.

46. Doedel EJ, Champneys A, Fairgrieve TF, Yu AB, Kuznetsov, A.P., Oldeman BE, et al. Auto-07p: Continuation and bifurcation software for ordinary differential equations [Internet]. 2007. Available from: http://cmvl.cs.concordia.ca/auto/

47. Szente MB, Boda B. Cellular mechanisms of neocortical secondary epileptogenesis. Brain Res. 1994 Jun 20;648(2):203–14.

48. Gilmore R, Morris H, Van Ness PC, Gilmore-Pollak W, Estes M. Mirror focus: function of seizure frequency and influence on outcome after surgery. Epilepsia. 1994;35(2):258–63.

49. Moran RJ, Stephan KE, Dolan RJ, Friston KJ. Consistent spectral predictors for dynamic causal models of steady-state responses. NeuroImage. 2011 Apr 15;55(4):1694–708.

50. Sheheitli H, Jirsa V. Incorporating slow NMDA-type receptors with nonlinear voltage-dependent magnesium block in a next generation neural mass model: derivation and dynamics [Internet]. bioRxiv; 2023 [cited 2023 Nov 23]. p. 2023.07.03.547465. Available from: https://www.biorxiv.org/content/10.1101/2023.07.03.547465v1

51. Marlin JJ, Carter AG. GABA-A Receptor Inhibition of Local Calcium Signaling in Spines and Dendrites. J Neurosci. 2014 Nov 26;34(48):15898–911.

52. Urban-Ciecko J, Barth AL. Somatostatin-expressing neurons in cortical networks. Nat Rev Neurosci. 2016 Jul;17(7):401–9.

53. Goldberg JH, Lacefield CO, Yuste R. Global dendritic calcium spikes in mouse layer 5 low threshold spiking interneurones: implications for control of pyramidal cell bursting. J Physiol. 2004 Jul;558(2):465–78.

54. Desroches M, Faugeras O, Krupa M. Slow-Fast Transitions to Seizure States in the Wendling-Chauvel Neural Mass Model. Opera Medica Physiol. 2015 Dec 1;2(3–4):228–34.

55. Lopez-Sola E, Sanchez-Todo R, Lleal È, Köksal-Ersöz E, Yochum M, Makhalova J, et al. A personalizable autonomous neural mass model of epileptic seizures. J Neural Eng. 2022 Sep;19(5):055002.

56. Kurbatova P, Wendling F, Kaminska A, Rosati A, Nabbout R, Guerrini R, et al. Dynamic changes of depolarizing GABA in a computational model of epileptogenic brain: Insight for Dravet syndrome. Exp Neurol. 2016 Sep;283:57–72.

57. Gnatkovsky V, Librizzi L, Trombin F, Curtis M de. Fast activity at seizure onset is mediated by inhibitory circuits in the entorhinal cortex in vitro. Ann Neurol. 2008;64(6):674–86.

58. Ben-Ari Y, Crepel V, Represa A. Seizures Beget Seizures in Temporal Lobe Epilepsies: The Boomerang Effects of Newly Formed Aberrant Kainatergic Synapses. Epilepsy Curr. 2008 May 1;8(3):68–72.

59. Ben-Ari Y, Dudek FE. Primary and Secondary Mechanisms of Epileptogenesis in the Temporal Lobe: There is a before and an After. Epilepsy Curr. 2010 Sep 1;10(5):118–25.

60. Mauritz M, Hirsch LJ, Camfield P, Chin R, Nardone R, Lattanzi S, et al. Acute symptomatic seizures: an educational, evidence-based review. Epileptic Disord. 2022;24(1):26–49.

61. Halász P, Bódizs R, Ujma PP, Fabó D, Szűcs A. Strong relationship between NREM sleep, epilepsy and plastic functions — A conceptual review on the neurophysiology background. Epilepsy Res. 2019 Feb 1;150:95–105.

62. Gelinas JN, Khodagholy D, Thesen T, Devinsky O, Buzsáki G. Interictal epileptiform discharges induce hippocampal-cortical coupling in temporal lobe epilepsy. Nat Med. 2016 Jun;22(6):641–8.

63. Dahal P, Ghani N, Flinker A, Dugan P, Friedman D, Doyle W, et al. Interictal epileptiform discharges shape large-scale intercortical communication. Brain. 2019 Nov 1;142(11):3502–13.

64. Yu H, Kim W, Park DK, Phi JH, Lim BC, Chae JH, et al. Interaction of interictal epileptiform activity with sleep spindles is associated with cognitive deficits and adverse surgical outcome in pediatric focal epilepsy. Epilepsia [Internet]. 2023 [cited 2023 Nov 24];n/a(n/a). Available from: https://onlinelibrary.wiley.com/doi/abs/10.1111/epi.17810

65. Khalife MR, Scott RC, Hernan AE. Mechanisms for Cognitive Impairment in Epilepsy: Moving Beyond Seizures. Front Neurol [Internet]. 2022 [cited 2022 Aug 22];13. Available from: https://www.frontiersin.org/articles/10.3389/fneur.2022.878991

66. Dallmer-Zerbe I, Jiruska P, Hlinka J. Personalized dynamic network models of the human brain as a future tool for planning and optimizing epilepsy therapy. Epilepsia. 2023;64(9):2221–38.

67. Jiruska P, Freestone D, Gnatkovsky V, Wang Y. An update on the seizures beget seizures theory. Epilepsia. 2023;00(n/a):1–12.

68. Berg AT, Shinnar S. Do Seizures Beget Seizures? An Assessment of the Clinical Evidence in Humans. J Clin Neurophysiol. 1997 Mar;14(2):102.

69. Kullmann DM, Lamsa KP. Long-term synaptic plasticity in hippocampal interneurons. Nat Rev Neurosci. 2007 Sep;8(9):687–99.

70. Honoré E, Khlaifia A, Bosson A, Lacaille JC. Hippocampal Somatostatin Interneurons, Long-Term Synaptic Plasticity and Memory. Front Neural Circuits [Internet]. 2021 [cited 2023 Jul 28];15. Available from: https://www.frontiersin.org/articles/10.3389/fncir.2021.687558

71. Zarnadze S, Bäuerle P, Santos-Torres J, Böhm C, Schmitz D, Geiger JR, et al. Cell-specific synaptic plasticity induced by network oscillations. Bartos M, editor. eLife. 2016 May 24;5:e14912.

72. Hadler MD, Tzilivaki A, Schmitz D, Alle H, Geiger JRP. Gamma-Oscillation Plasticity Is Mediated by Parvalbumin Interneurons [Internet]. bioRxiv; 2023 [cited 2023 Aug 25]. p. 2023.06.21.545901. Available from: https://www.biorxiv.org/content/10.1101/2023.06.21.545901v1

73. Litwin-Kumar A, Doiron B. Formation and maintenance of neuronal assemblies through synaptic plasticity. Nat Commun. 2014 Nov 14;5(1):5319.

74. Abraham WC, Jones OD, Glanzman DL. Is plasticity of synapses the mechanism of long-term memory storage? Npj Sci Learn. 2019 Jul 2;4(1):1–10.

75. Bikbaev A, Manahan-Vaughan D. Relationship of hippocampal theta and gamma oscillations to potentiation of synaptic transmission. Front Neurosci [Internet]. 2008 [cited 2023 Mar 2];2. Available from: https://www.frontiersin.org/articles/10.3389/neuro.01.010.2008

674 Figure 1

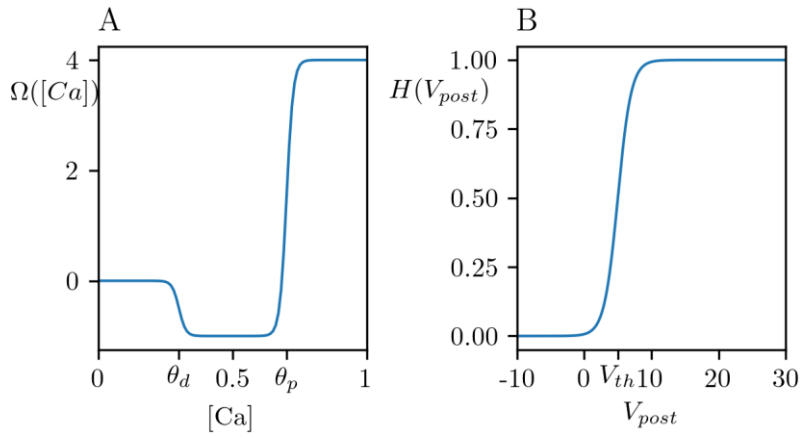

675

676

677 Figure 2

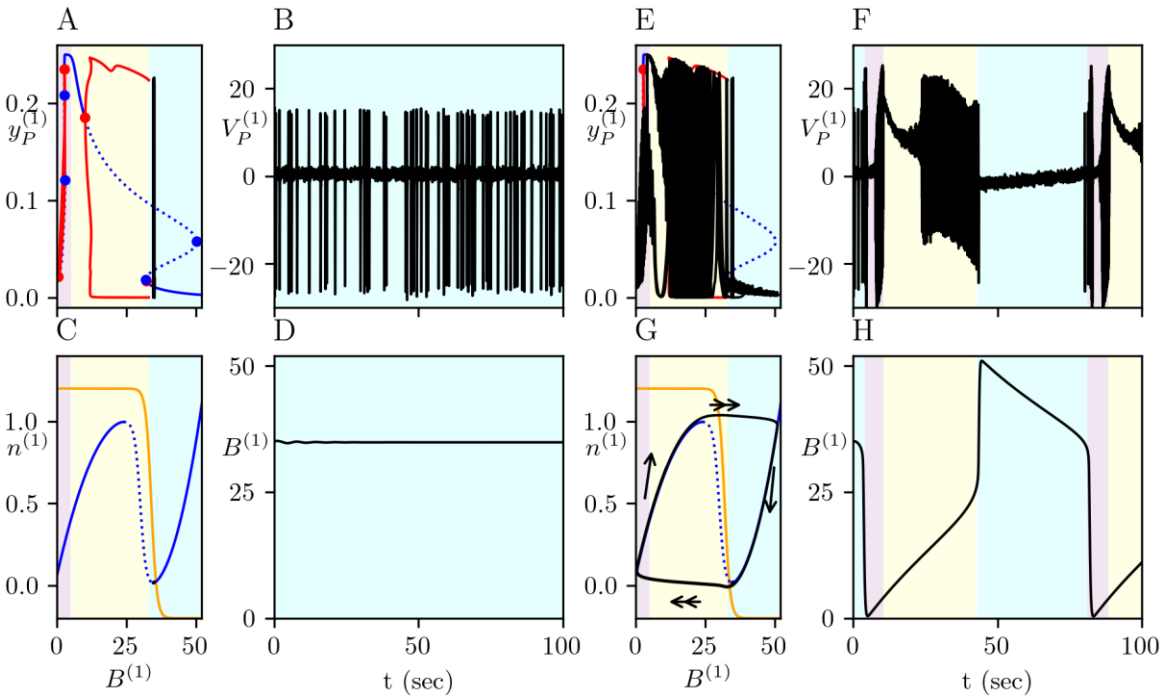

678

679

680

681

682 Figure 3

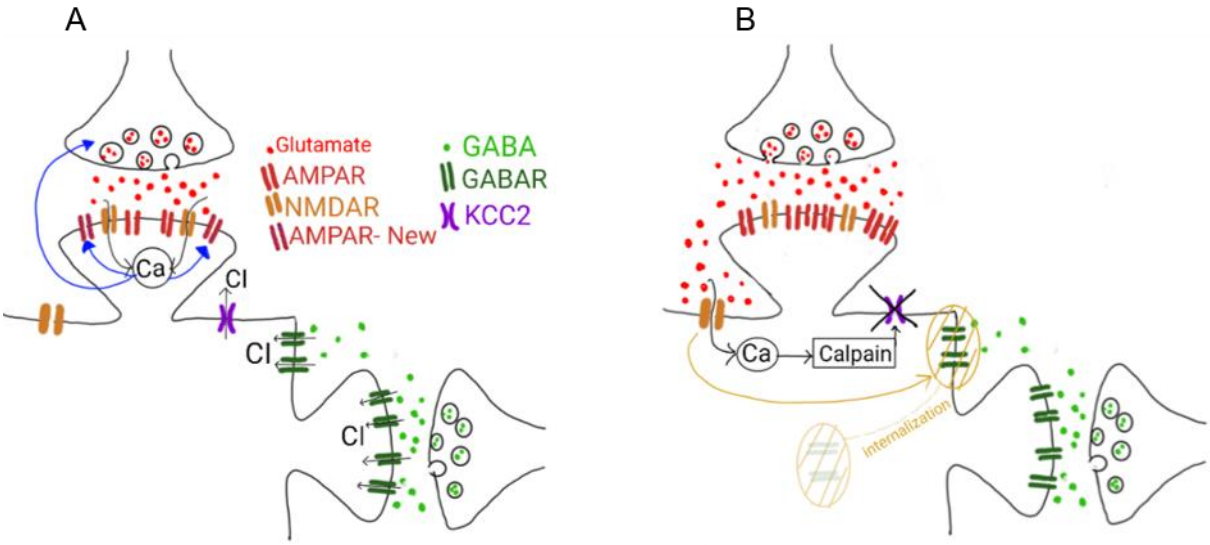

683

684

685

686

687

688

689

690

691

692

693

694

695

696

697 Figure 4

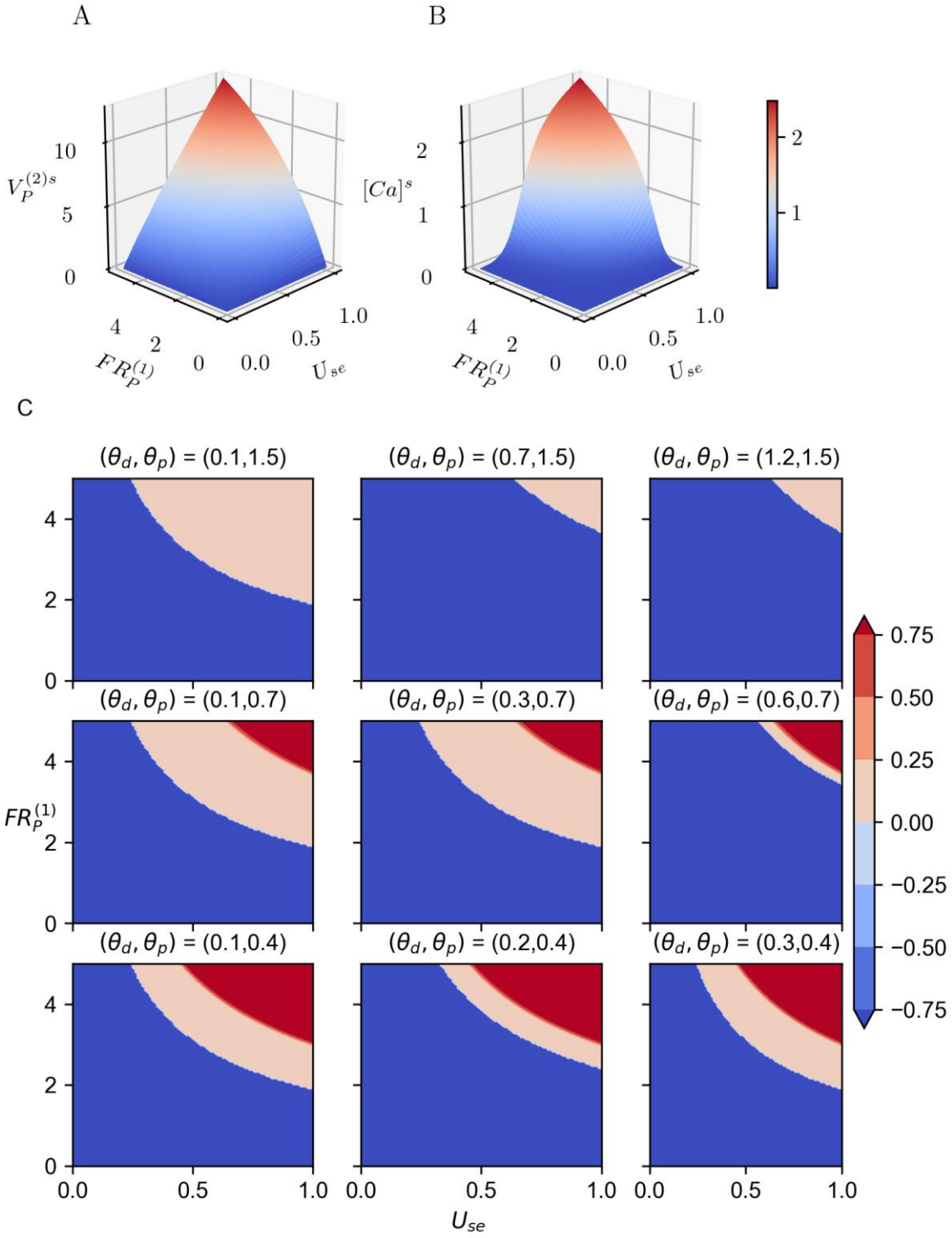

698

699

700

Figure 5

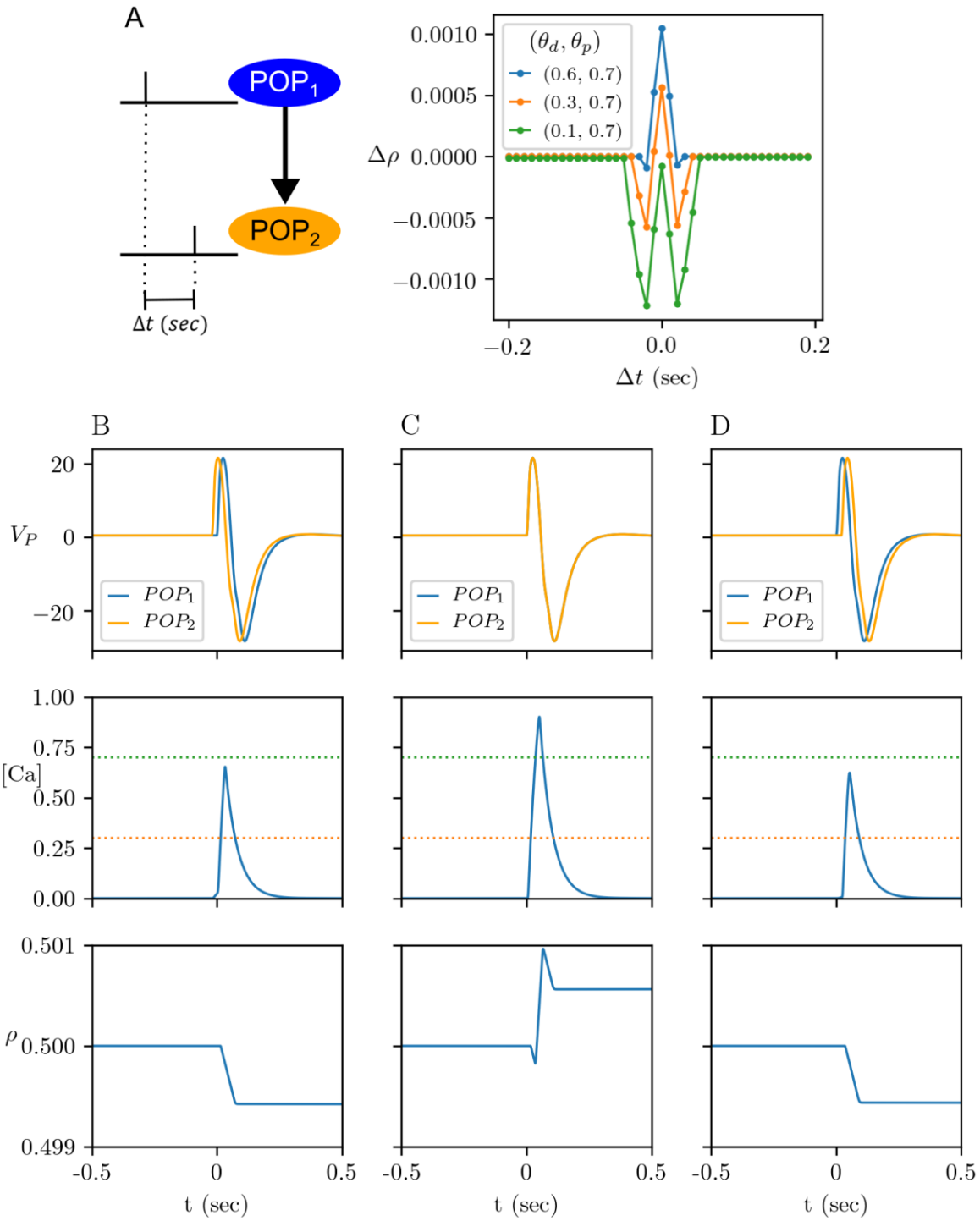
A
POP1
POP2
Δt (sec)
0.0010
0.0005
Δρ 0.0000
−0.0005
−0.0010
(θd, θp)
(0.6, 0.7)
(0.3, 0.7)
(0.1, 0.7)
−0.2
0.0
0.2
Δt (sec)
B
C
D
20
VP 0
−20
POP1
POP2
1.00
0.75
[Ca]
0.50
0.25
0.00
0.501
ρ 0.500
0.499
-0.5
0
0.5
t (sec)

706 Figure 6

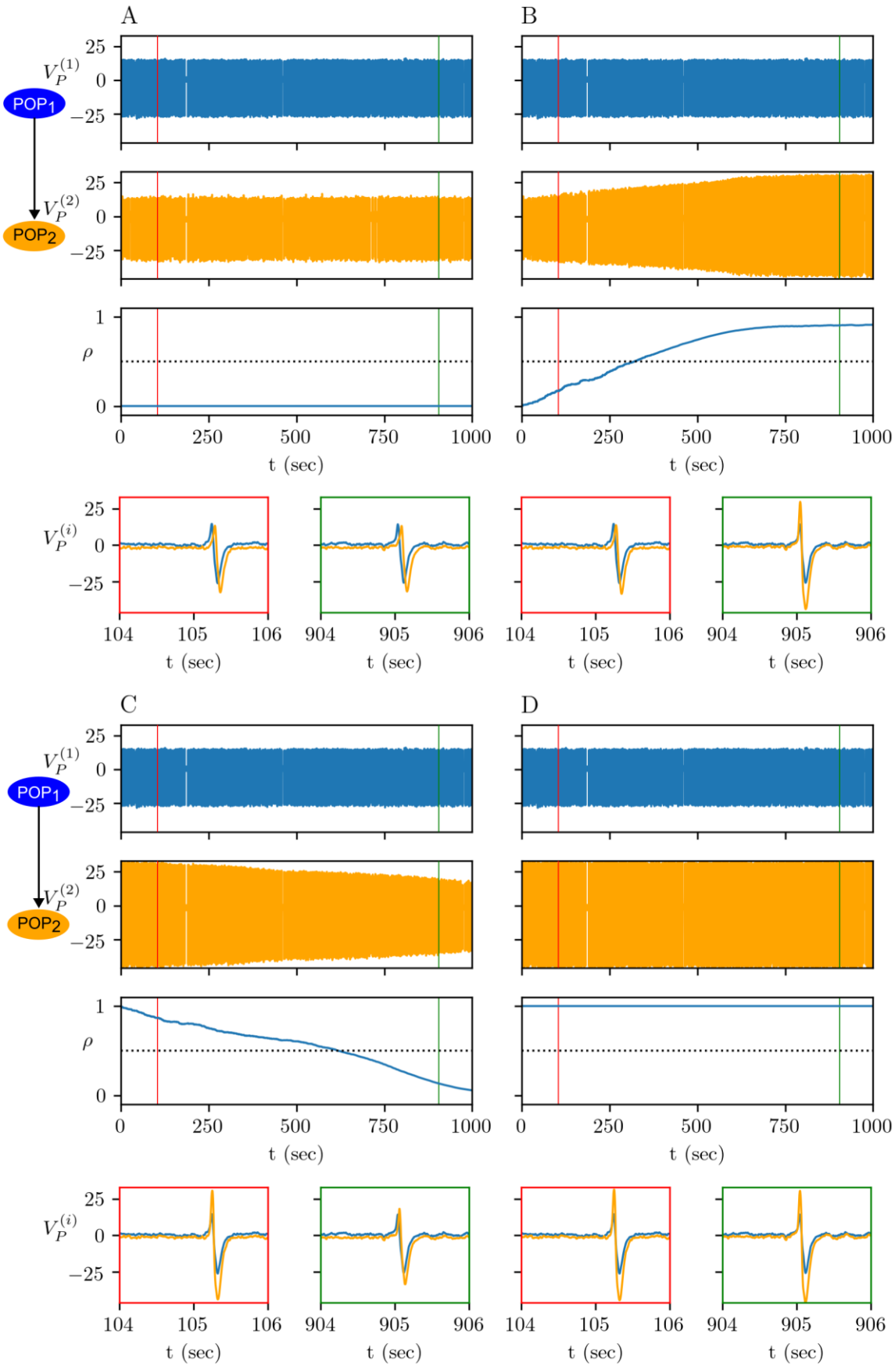

707

708 Figure 7

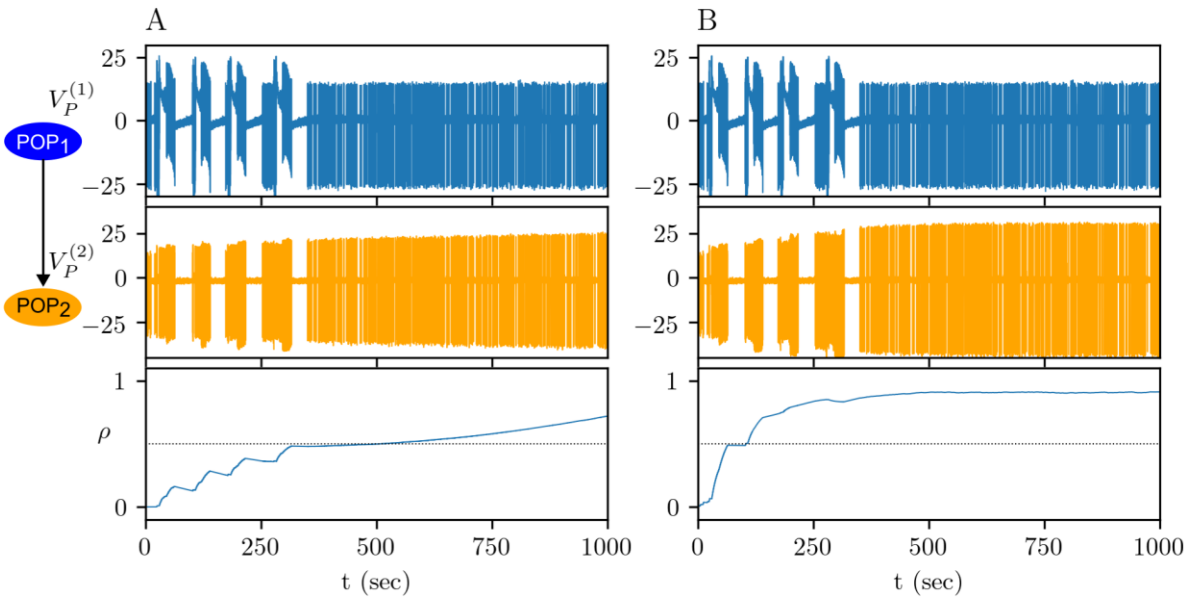

709

710 Figure 8

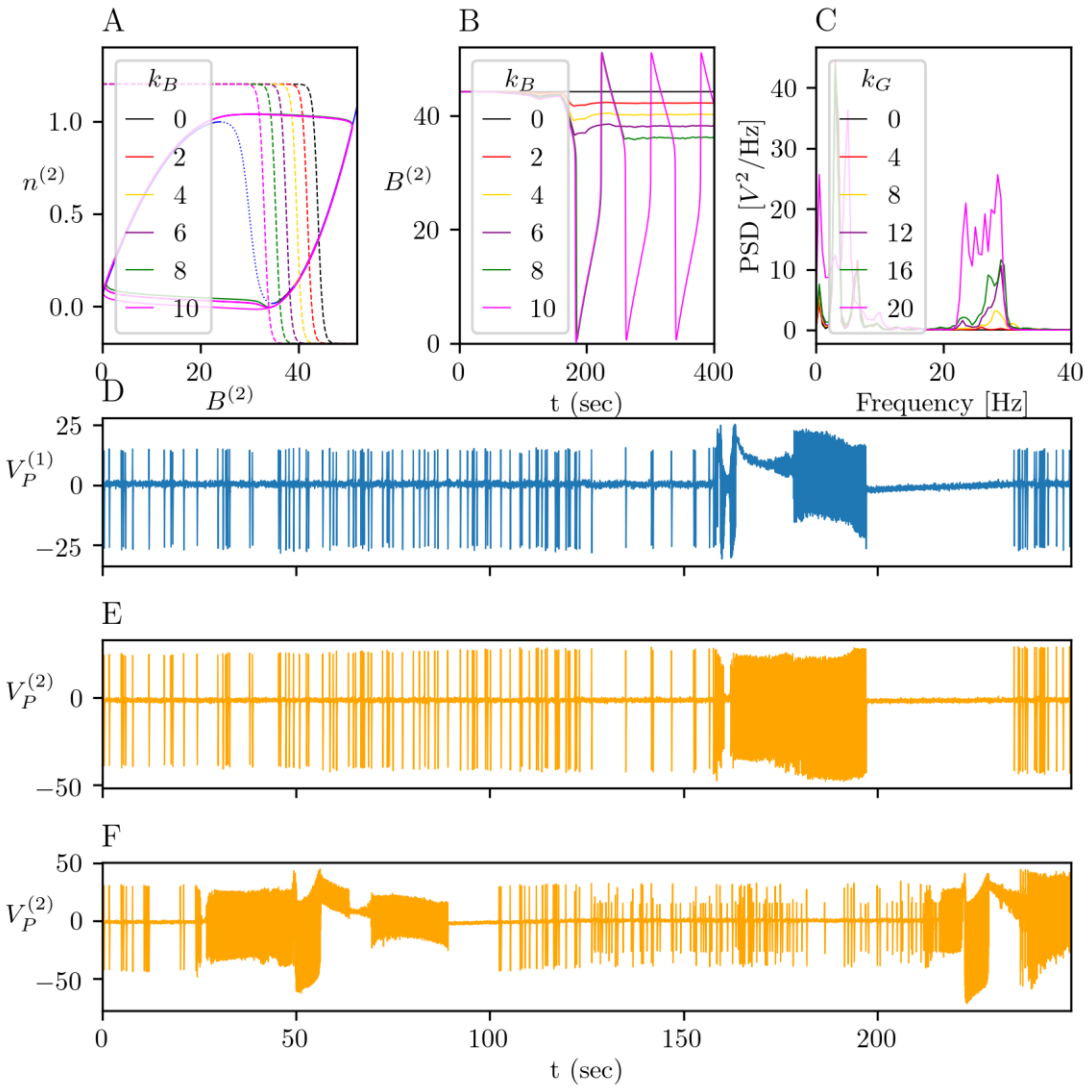

711

712

713

714

715

716

717 Figure 9

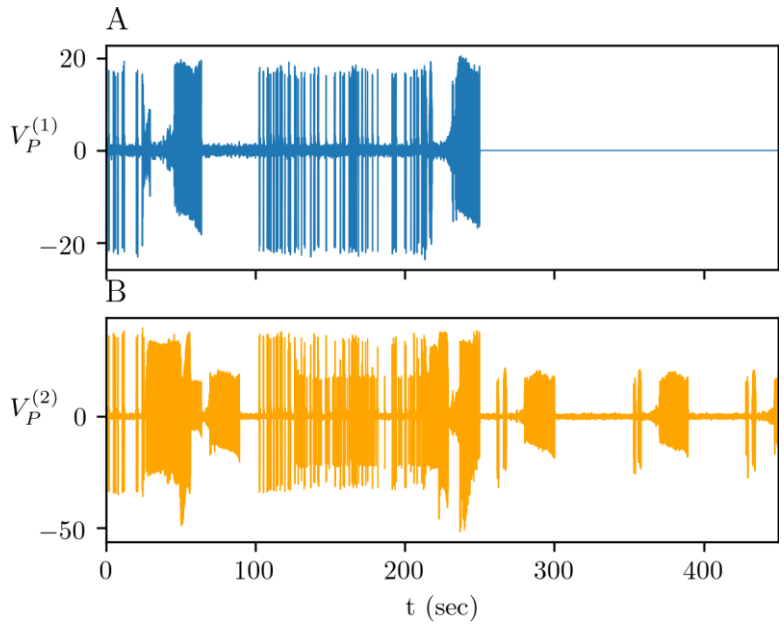

718

719